15TH IEA HEAT PUMP CONFERENCE
MAY 26–29, 2026 | HOFBURG
VIENNA 2026
DECARBONISATION THROUGH INNOVATION

Experimental investigation of hydrocarbon refrigerant leakage under varying conditions

Jafar Esmaeelian[a*], Björn Palm[a], Rahmatollah Khodabandeh[a], Hatef Madani[a]

[a] KTH Royal Institute of technology, Stockholm, Sweden

Abstract

Accurate quantification of refrigerant leakage is critical for evaluating the safety risks associated with hydrocarbon refrigerants such as R-290. This study presents an experimental investigation of R-290 leakage rates through holes of different diameters representative of potential failure scenarios in refrigeration and heat-pump systems. In this article, a weighing method is employed to directly measure the mass loss from a simplified containment setup, enabling time-resolved characterization of leakage behaviour under controlled liquid and vapor conditions. The results demonstrate clear differences between liquid- and gas-phase leaks, driven by transient cooling, pressure drop, and phase-change effects. These insights contribute to more accurate leakage-source modelling, support the refinement of charge-limit guidelines, and inform the development of effective mitigation strategies for the safe use of flammable refrigerants.

Keywords: Refrigeration, Safety, Leakage, Propane

1. Introduction

The global transition toward low-GWP refrigerants has increased the use of hydrocarbons such as R-290 in air-conditioning and refrigeration systems. While these refrigerants offer clear environmental benefits, their flammability demands a thorough understanding of leakage behavior, since the rate and nature of a refrigerant release strongly influence flammability risk, charge-limit development, and the design of mitigation strategies.

Previous studies have reported differing conclusions on the relative severity of vapor versus liquid leaks. Experiments at Oak Ridge National Laboratory (ORNL), conducted as part of the AHRTI 9012 program, showed that under equal upstream saturation temperature and pressure conditions, liquid leaks can discharge up to seven times faster than vapor leaks, primarily due to the higher density of liquid refrigerant at the same pressure [1]. However, other observations from the same program suggested that the difference may be more modest under certain conditions. In compressor-off scenarios, for example, refrigerant redistribution through the expansion device led to two-phase discharge from nominally low-pressure sections, allowing low-side leaks to release comparable fractions of the total charge as high-side leaks [1].

Similar outcomes have been reported in large collaborative projects such as AHRTI 9007-01 and 9007-02, where full HVAC and refrigeration systems were tested under controlled leak scenarios [2]. These investigations concluded that leak severity depends not only on whether liquid or vapor is discharged, but also on leak location, system elevation, internal volumes, and equipment configuration. In several cases, ignition behavior was found to correlate more strongly with release geometry and mixing conditions than with refrigerant phase alone. Furthermore, laboratory measurements of R-290 leakage mass-flow rates have shown that discharge coefficients and orifice geometry play a dominant role in determining flow behavior, without consistently indicating dramatic differences between liquid and vapor leakage under all conditions [3].

This divergence in reported findings illustrates a key uncertainty in current safety assessments: whether it is appropriate to assume that liquid leaks always dominate, or whether more nuanced correlations—accounting for geometry, thermodynamic state, and transient behavior—are required. Importantly, most prior studies were performed using full HVAC systems, where refrigerant migration, internal line volumes, and heat-exchanger interactions can obscure the fundamental leakage mechanism. To address this limitation, the present work uses a simplified and well-controlled dual-cylinder apparatus designed to isolate vapor and liquid leakage conditions without the confounding effects of system operation.

The primary objective of this study is to provide accurate, experimentally measured leakage rates for R-290 under conditions representative of potential failure scenarios in air-conditioning and heat-pump systems. By systematically varying the hole diameter and monitoring the time-resolved mass loss with a precision weighing method, the study aims to (i) establish reliable leakage-rate data for hydrocarbon refrigerants, (ii) evaluate how hole size influences leakage dynamics, and (iii) compare the results with existing literature that has reported both significant and modest differences between liquid and vapor releases. These measurements are intended to supply critical input to CFD modeling efforts, refine charge-limit formulations in safety standards, and support the development of effective mitigation strategies for the safe use of flammable refrigerants.

2. Method

2.1. Experimental setup

Figure 1 shows the experimental setup used to investigate the refrigerant leakage rate and thermal behavior of R-290 under controlled conditions. The setup consists of two vertically mounted stainless-steel cylinders connected by high-pressure stainless-steel tubing. The upper cylinder represents the gas side of a heat pump system, while the lower one represents the liquid side. Both cylinders are placed on an electronic balance (±1 g accuracy, 10 Hz logging frequency) to continuously monitor the total mass loss during leakage.

Each cylinder is equipped with pressure and temperature sensors installed close to the potential leak points to measure the instantaneous thermodynamic state of the refrigerant. A service port is included for evacuation and charging. The outlet valves of the cylinders are fitted with interchangeable orifice fittings to simulate leaks of different sizes. In this study, three orifice diameters were tested: 0.3 mm, 0.5 mm and 1.0 mm.

The entire system is placed outside to ensure safe discharge of the leaked propane. The test rig is designed to safely contain up to 300g of R-290 with a maximum operating pressure of 20 bar.

a)

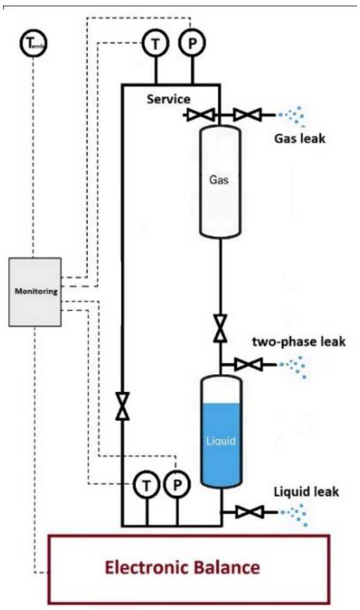

b)

Figure 1. Test setup overview: a) schematic diagram, b) constructed test rig.

2.2. Test procedure

Before each test, the rig was evacuated to below 2 mbar using a vacuum pump and then charged with the desired mass of R-290. The system was allowed to stabilize to ambient temperature before initiating the leakage test. Three leak positions were defined along the vertical axis of the setup to represent different fluid conditions:

1. Gas leak (upper port): simulating a vapor-phase leak.
2. Mid-level port: representing a partially liquid, partially vapor discharge.
3. Liquid leak (bottom port): simulating a leak from the liquid side.

Each test was initiated by opening the corresponding valve while logging pressure, temperature, and mass data simultaneously. The leakage continued until the system pressure equalized with ambient conditions or until the entire refrigerant charge was released.

2.3. Infrared imaging

To observe the thermal behaviour of the system during leakage, an infrared (IR) camera was positioned to capture the entire cylinder assembly. The IR images provided spatial and temporal temperature distributions over the cylinder surfaces, allowing visualization of cooling effects caused by refrigerant evaporation and flashing. This information was used to identify temperature gradients between the gas and liquid regions and to validate the pressure–temperature relationships observed in the sensor data.

2.4. Data analysis

The mass flow rate of the refrigerant was obtained by differentiating the measured mass data over time. The leakage rate was then correlated with the upstream pressure and fluid phase. For each leak position, tests were repeated for three orifice diameters (0.3 mm, 0.5 mm and 1.0 mm) to assess the effect of hole size on leakage rate and temperature evolution. The data obtained were compared against theoretical orifice-flow correlations for both liquid and vapor leakage conditions.

The uncertainty of the mass loss measurement is primarily governed by the resolution and sampling rate of the electronic balance. For the present setup, the mass uncertainty is small relative to the total discharged mass, and its effect on the calculated leakage rate is most pronounced during the very early stages of rapid liquid discharge. Leakage rates derived during slower vapor-phase discharge are less sensitive to measurement noise. In addition, while individual test conditions were not repeated systematically, the observed pressure decay, mass-loss evolution, and leakage-rate trends were consistent across different orifice sizes and leak locations. This consistency provides confidence in the robustness of the reported leakage behaviour.

2.5. Limitations

It should be noted that the present experiments were conducted using a simplified dual-cylinder geometry. While this approach enables clear interpretation of phase-dependent leakage behavior, the absolute leakage rates reported here should not be directly extrapolated to full air-conditioning or heat-pump systems. In real equipment, additional factors such as complex internal geometries, distributed refrigerant inventory, oil presence, and component-level heat transfer can influence leakage dynamics. The results should therefore be interpreted as representative of underlying physical trends rather than system-specific leakage magnitudes.

3. Results and Discussion

3.1. System pressure loss

Figure 2 shows the measured pressure decay for the top-hole (gas-side) leakage tests for hole diameters of 0.3 mm, 0.5 mm, and 1.0 mm. The results also include the mid-level 0.5 mm leakage test, which initially exhibits a short two-phase discharge but transitions to gas-phase flow. Because the majority of pressure decay follows vapor-phase behaviour, this case is grouped with the top-hole results (For the final version of the paper, we will repeat the tests for the 0.3 mm hole, as the ambient temperature during those experiments differed from the other test conditions).

For all gas-phase tests, the pressure decreases smoothly with a characteristic exponential-like decay typical of choked or near-choked compressible flow. As expected, the smallest orifice (0.3 mm) leads to the slowest pressure reduction, requiring more than 4800 s to reach atmospheric pressure. In contrast, the 1.0 mm orifice results in a rapid pressure drop, reaching near-equilibrium conditions around 800 s.

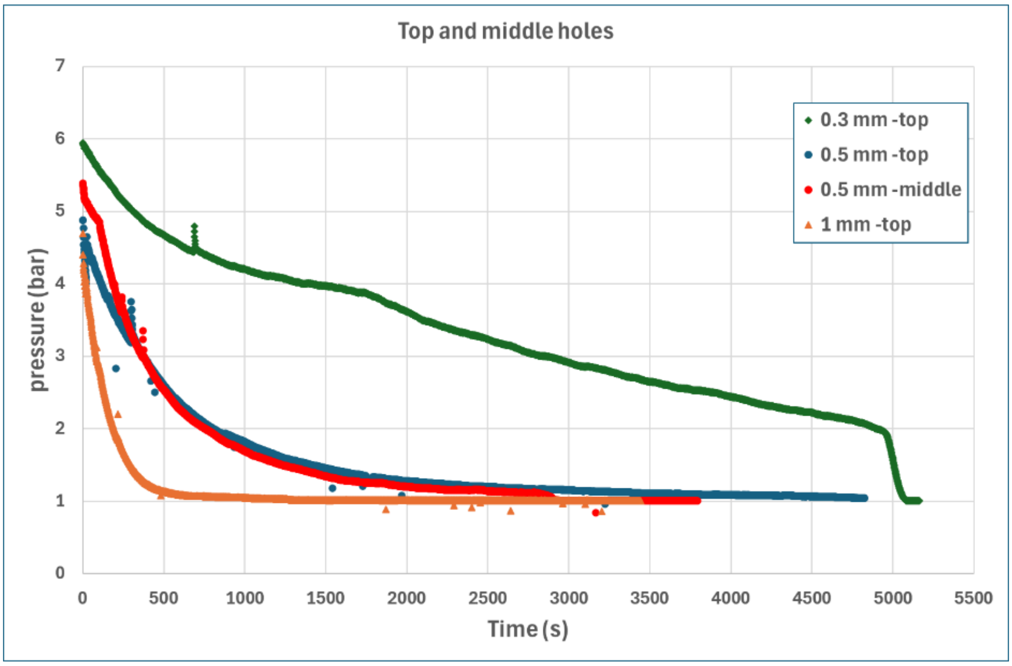

Figure 2. Pressure decay for gas-side leakage (top hole) for hole diameters of 0.3 mm, 0.5 mm, and 1.0 mm

Figure 3 presents the corresponding pressure loss for the bottom-hole (liquid-side) leakage tests. In all cases, liquid leaks exhibit a significantly faster pressure decline due to the higher fluid density. The pressure drop is characterized by sharp inflection points that reflect transitions between liquid, two-phase, and vapor discharge as the internal mass inventory changes. For the 1.0 mm orifice, full depressurization occurs within 80–120 s, while the 0.3 mm orifice extends the duration to approximately 500 s.

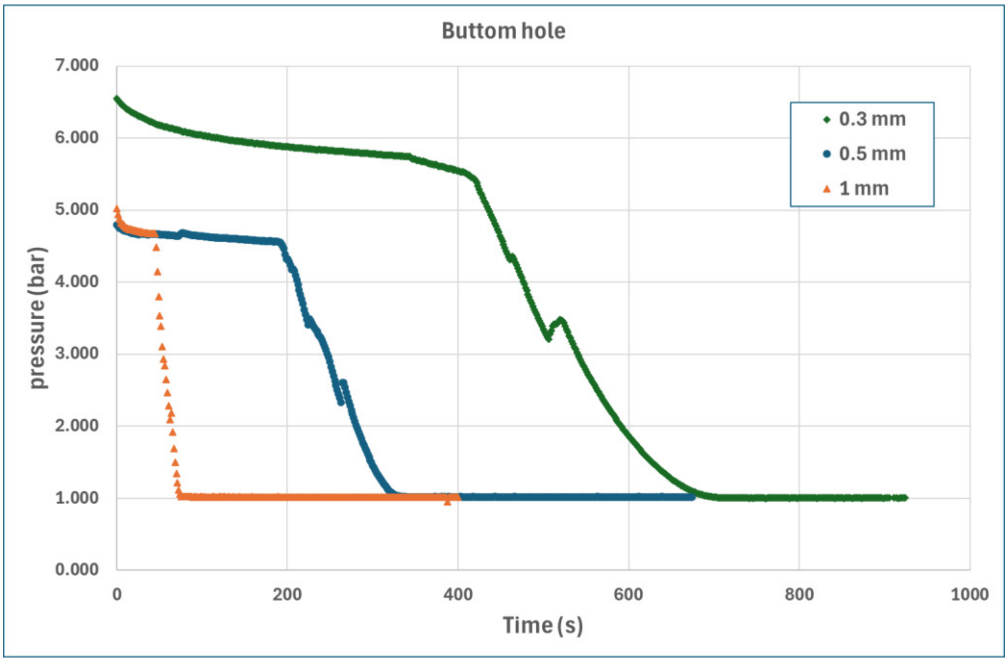

Figure 3. Pressure decay for liquid-side leakage (bottom hole) for hole diameters of 0.3 mm, 0.5 mm, and 1.0 mm

Comparing the gas- and liquid-side tests demonstrate the strong influence of fluid phase on pressure-decay dynamics. Liquid leaks exhibit rapid depressurization driven by high mass flux and flashing, whereas gas leaks show a slower, smoother pressure decline governed by compressible-flow limitations. The mid-level leakage case falls between these two behaviors but aligns more closely with the gas-phase trend after the initial flashing period.

3.2. 3.2 Leaked mass

Figure 4 presents the cumulative leaked mass for all seven test conditions, covering gas-phase leakage from the top port, liquid-phase leakage from the bottom port, and the mid-level 0.5 mm case. The results clearly show that the phase of the refrigerant at the leak location has a dominant influence on the overall discharge behavior.

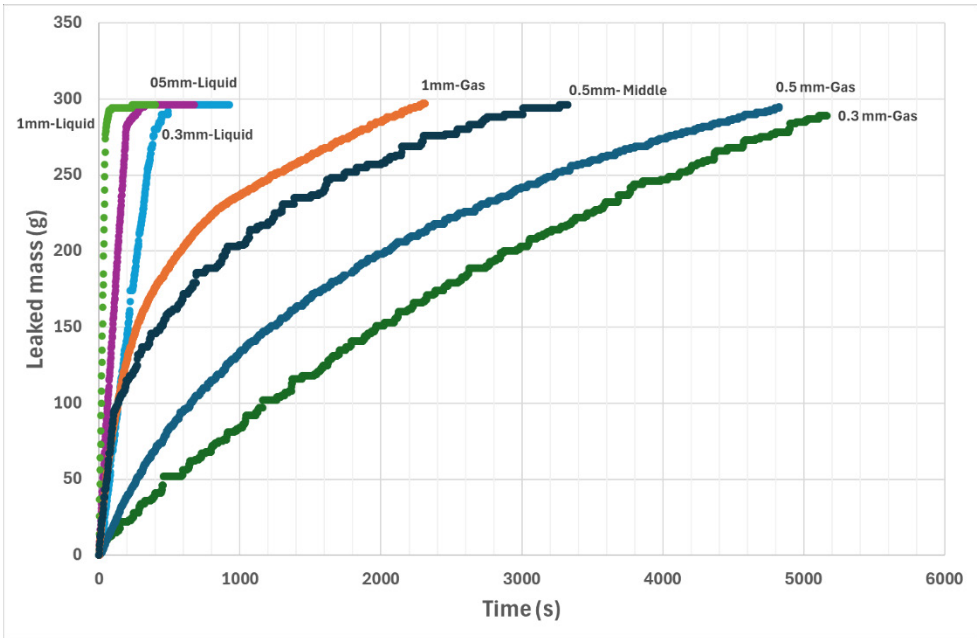

Figure 4. Cumulative leaked mass for gas-phase, liquid-phase, and two-phase leakage conditions for different orifice diameters

The liquid-side tests exhibit the fastest mass release. Because liquid R-290 has a much higher density and undergoes flashing as it experiences a sharp pressure drop across the orifice, the discharge is extremely rapid. The 1.0 mm liquid leak releases almost the entire refrigerant charge within only 90 s, while the 0.5 mm liquid leak reaches full discharge in 360 s. The smallest orifice, 0.3 mm, empties the system in roughly seven minutes. These rapid increases in leaked mass are consistent with the steep pressure drops previously observed in the liquid-phase measurements.

In contrast, the gas-side leakage cases show a much more gradual release of mass. The 1.0 mm gas leak requires 2300 s to fully discharge the charge, while the 0.5 mm gas leak reaches that point after approximately 4800 s. The slowest case is the 0.3 mm gas leak, which takes more than 5000 seconds to release the full amount. This slower progression reflects the lower density of vapor R-290 and the compressible-flow limitations on mass flux through small orifices.

The mid-level 0.5 mm leak presents an intermediate behaviour. At the beginning of the test, the refrigerant at this height contains some liquid, resulting in a short period of rapid two-phase discharge and a steep initial rise in leaked mass. However, once this liquid fraction is depleted, the flow transitions to vapor-phase leakage, and the cumulative mass curve closely follows the profile of the corresponding gas-phase case for most of the test duration. This confirms that the dominant discharge mechanism during the majority of the test is gaseous rather than liquid. Overall, the results demonstrate that the phase of the refrigerant at the leak point is the primary factor determining the leakage dynamics, with hole size acting as a secondary influence.

Figure 5 and 6 compares the experimentally measured leakage rate for the 0.3 mm orifice with theoretical predictions for both liquid and vapor discharge respectively. The leakage rate was derived by differentiating the cumulative mass-loss data and applying a moving-average filter to reduce noise. The resulting curves capture the strong dependence of mass flux on the thermodynamic state of the refrigerant and the transient cooling of the cylinder during discharge.

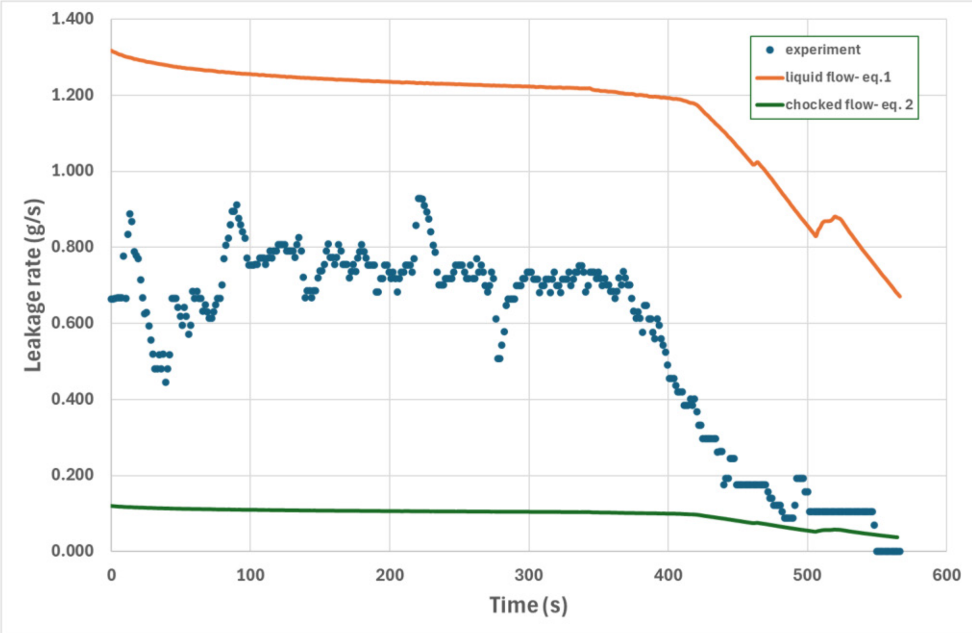

Figure 5. Measured leakage rate for the 0.3 mm liquid-phase test compared with theoretical models

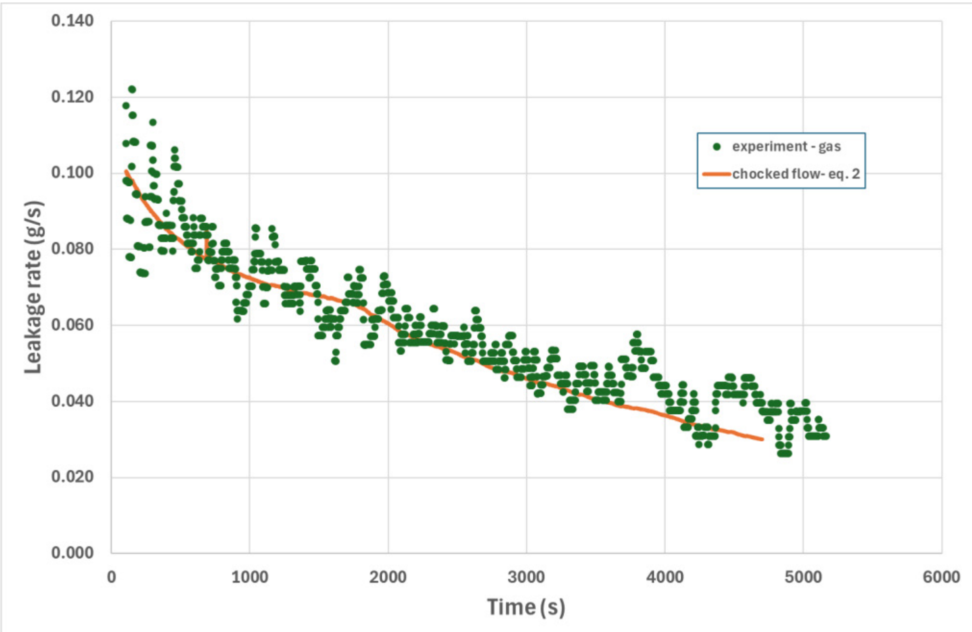

Figure 6. Measured leakage rate for the 0.3 mm gas-phase test compared with the choked-flow theoretical model.

For the liquid-side case, the theoretical leakage rate was calculated using the standard incompressible orifice equation:

The liquid leakage rate was calculated using the standard incompressible orifice equation [4], which has been widely applied in refrigerant leak studies, including AHRTI and ORNL programs.

$$\dot{m} = C_d A_0 \sqrt{2\rho_\ell (p_0 - p_{atm})} \tag{1}$$

Where:

$\dot{m}_\ell$ is the mass flow in g/min;
C_d is the discharge coefficient (set to 0.61);
A_0 is the leak hole area;
ρ_l is the upstream liquid density in kg/m3;
p_0 is the vapour pressure in Pa of refrigerant vapour at the applicable dew point temperature;
p_{atm} is the atmospheric pressure 1.0132 5 ×105 in Pa.

A discharge coefficient of $C_d = 0.85$ was selected, consistent with values recommended for sharp-edged orifices in refrigerant leakage studies.

The liquid mass flow rate remains nearly constant in the early part of the test because both the density and upstream pressure vary only slightly. As can be seen, Eq. (1) overpredicts the mass flux, since the incompressible model does not account for flashing and vapor formation at the hole. Although the leak originates from a region containing liquid refrigerant, the outflow does not remain a pure liquid jet. The sudden pressure drop from the internal saturation pressure (5–7 bar) to atmospheric pressure causes the liquid R-290 to flash immediately at the orifice, producing a two-phase mixture of vapor and liquid droplets. As a result, the discharge rapidly transitions from liquid-like behaviour to compressible, two-phase flow. This flashing reduces the effective density and mass flux of the escaping refrigerant compared with a true incompressible liquid stream. Therefore, the classical incompressible orifice equation, which assumes single-phase liquid flow, tends to overestimate the leakage rate once flashing begins.

For the gas-side leakage, the theoretical prediction was obtained using the standard choked-flow equation for compressible gases [5]:

$$\dot{m}_g = 0.06\, C_d A_0 \sqrt{k\rho_0(p_0 - p_{atm})\left(\frac{2}{k+1}\right)^{\frac{k+1}{k-1}}} \tag{2}$$

Where:

$\dot{m}_g$ is the mass flow in g/min;
C_d is the discharge coefficient (set to 0.61);
A_0 is the leak hole area;
k is the ratio of specific heats of refrigerant vapour at the applicable dew point temperature;
ρ_0 is the density in kg/m3 of refrigerant vapour at the applicable dew point temperature;
p_0 is the vapour pressure in Pa of refrigerant vapour at the applicable dew point temperature;
p_{atm} is the atmospheric pressure 1.0132 5 ×105 in Pa.

Because the upstream-to-downstream pressure ratio almost always exceeded the critical value during the test, the leak operated under choked-flow conditions for nearly the entire event. As a result, the predicted mass flow rate decreases gradually as the cylinder cools and depressurizes, and the experimental gas leakage rate closely follows the theoretical curve after the initial transient.

In contrast, the experimentally measured liquid leakage rate is an order of magnitude higher than the gas leakage rate under the same initial pressure. For the 0.3 mm orifice, the vapor leakage rate ranges from approximately 0.06 to 0.10 g/s, while the liquid leakage rate stabilizes around 0.7–0.9 g/s during the early part of the test. This strong phase dependence aligns with the findings of previous ORNL studies, which reported liquid mass fluxes up to 7 times higher than vapor mass fluxes at similar upstream conditions [1].

Even in liquid leakage, as the pressure decreases and flashing occurs at the orifice, the flow rapidly transitions to a two-phase regime, and the incompressible liquid orifice equation increasingly overpredicts the measured mass flow rate. In contrast, the choked gas-flow model accurately captures vapor-phase leakage once the discharge becomes vapor-dominated but is not intended to represent early-time liquid flashing behaviour. These observations highlight the importance of accounting for phase transition and transient thermodynamic effects when applying simplified leakage models.

Overall, the comparison between experimental and theoretical leakage rates demonstrates that vapor discharge is well represented by standard choked-flow models, while liquid discharge requires consideration of flashing and two-phase flow to accurately capture the observed mass flux.

3.3. Temperature change

Figure 7 shows the temperature evolution captured by infrared (IR) imaging for gas-phase and liquid-phase leakage. The IR data reveals how the thermal behavior inside the cylinders is governed by evaporation dynamics, liquid level movement, and the interaction between flashing and internal heat transfer.

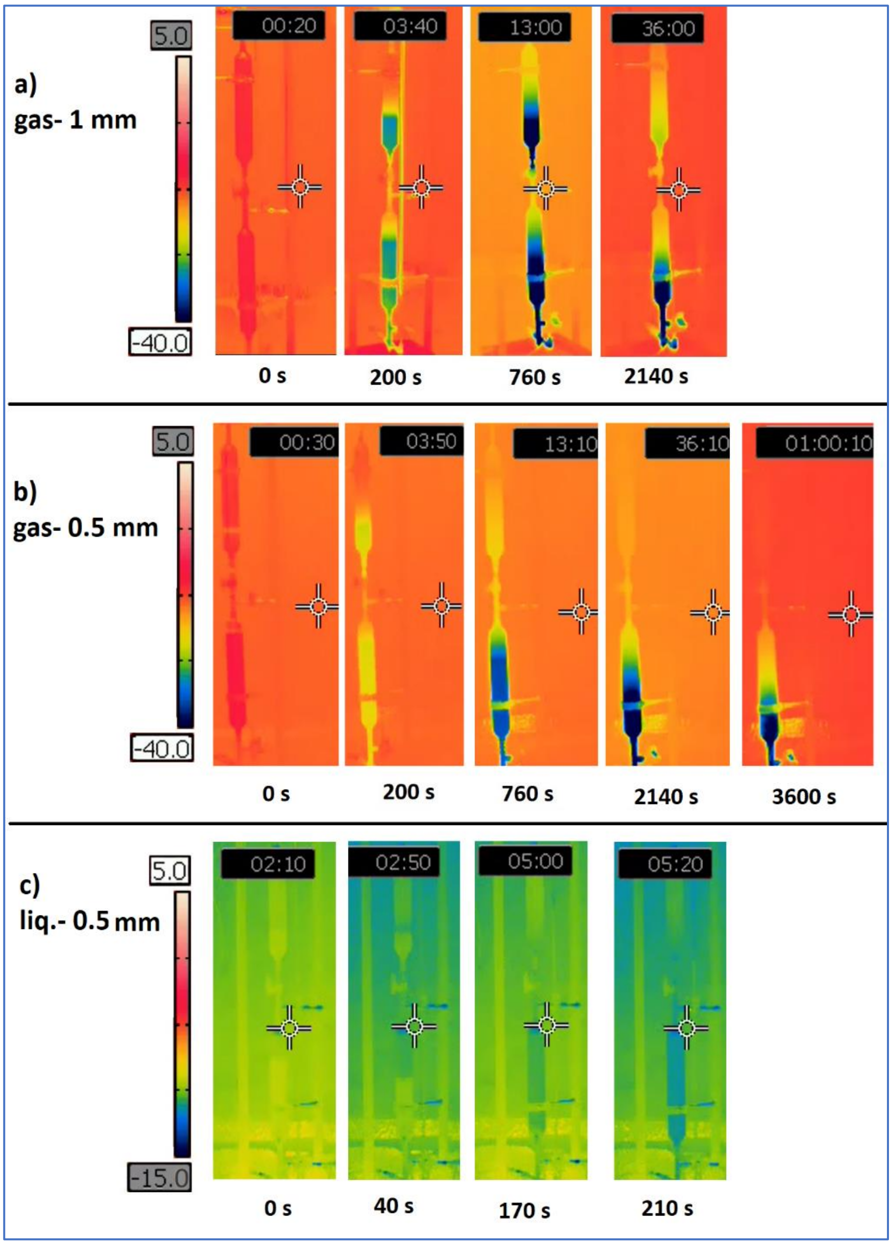

Figure 7. Infrared temperature evolution during (a) gas leakage through a 1 mm orifice, (b) gas leakage through a 0.5 mm orifice, and (c) liquid leakage through a 0.5 mm orifice.

For the gas-phase leaks (1 mm and 0.5 mm holes), the cooling pattern progresses gradually and follows the depressurization trend. As the pressure decays, the vapor temperature decreases, and this cooling is transmitted through the cylinder wall. After the leak begins, the coldest region appears around the liquid reservoir inside the lower cylinder, especially at the liquid–vapor interface. This is expected because evaporation occurs predominantly at the liquid surface, where latent heat must be absorbed to sustain boiling as pressure decreases. The 1 mm gas leak shows a steeper and more pronounced cooling compared to the 0.5 mm case because of its faster pressure drop. However, the overall cooling remains moderate, consistent with the relatively low mass flow rate and the absence of liquid flashing in these conditions.

In the 1 mm gas-leak case, a unique phenomenon is observed: a part of colder liquid appears to travel upward from the lower cylinder into the upper cylinder. This indicates that the rapid depressurization and internal turbulence cause liquid splashing into the vapor region, where it evaporates after contacting the warmer upper wall.

The liquid leak behaves differently. Although the total mass is discharged very rapidly and the instantaneous leak rate is much higher, a large fraction of the liquid leaves the cylinder without evaporating inside. Most of the flashing and evaporation occur in the external jet after the liquid passes through the orifice. Consequently, the amount of latent heat taken from the cylinder wall is comparatively small, and the internal cooling is less pronounced than in the gas tests. The IR images for the 0.5 mm liquid leak show only a moderate drop in surface temperature confined mainly to the lower cylinder, and the cooling quickly disappears once the liquid inventory is exhausted, and the leak stops after a short time.

Overall, the IR measurements demonstrate that internal evaporation, not total discharged mass, governs the cooling of the cylinders. Gas leaks produce sustained internal evaporation during the long depressurization period and therefore lead to stronger and more widespread cooling. In contrast, liquid leaks discharge a large amount of refrigerant very quickly, but much of the phase change occurs outside the vessel, so the internal temperature drop is comparatively limited.

4. Conclusions

This study presented controlled measurements of liquid and vapor R-290 leakage through different hole sizes using a simplified dual-cylinder apparatus. The results show that liquid leaks initially produce much higher mass fluxes than vapor leaks of the same hole diameter due to the higher effective density at the leakage point. However, the liquid mass flow does not remain constant; instead, it rapidly decreases as the cylinder cools, the internal pressure drops, and a significant portion of the phase change occurs outside the vessel. Gas-phase leaks exhibit much lower instantaneous mass fluxes but generate stronger internal cooling because evaporation takes place predominantly inside the cylinder during a prolonged depressurization period. In all cases, the leakage rate evolves dynamically as a result of the tight coupling between mass flow, internal evaporation, and heat transfer from the surroundings.

These observations emphasize that leak rates cannot be accurately represented by models assuming constant upstream pressure or steady discharge conditions. The transient pressure drop, and associated temperature decrease substantially reduce the leak rate over time compared with constant-pressure predictions. Consequently, models that neglect internal cooling effects may overestimate the severity or duration of vapor cloud formation.

While the experimental trends are robust, the magnitude of the leak rates is influenced by heat transfer into the test cylinders, ambient conditions, and the simplified geometry used in this work. Therefore, the results should not be interpreted as universally representative of all system configurations. Nonetheless, the fundamental behavior, rapid early discharge for liquid leaks, sustained evaporation for vapor leaks, and the strong dependence of leak rate on internal cooling provides valuable guidance for refining leakage models used in standards such as IEC 60335-2-89. In addition, from a safety-standards perspective, the present results support the use of choked-flow-based source-term models, as adopted in IEC 60335-2-89, for representing high-pressure refrigerant leaks. However, the measurements also show that internal cooling, pressure decay and refrigerant outlet density significantly affect the leakage rate over time compared with gaseous constant-pressure assumptions. Incorporating such transient effects into leakage modeling can improve estimates of released mass and resulting refrigerant concentrations, potentially reducing unnecessary conservatism while maintaining safety margins. Future work should extend these measurements to more complex geometries, varying thermal environments, and systems containing oil to further improve the predictive accuracy of refrigerant leak models.

Acknowledgements

Authors wish to acknowledge the financial support of “Energimyndigheten” under Grant No. P2022-00473. Additionally, the computations processing was enabled by resources provided by the National Academic Infrastructure for Supercomputing in Sweden (NAISS), partially funded by the “Swedish Research Council” through grant agreement No. 2022-06725.

References

[1] V. R. Baxter, W. Miller, A. Abu-Heiba, et al., Refrigerant Leak and Ignition Testing for Flammable Refrigerants (AHRTI 9012), ORNL/TM-2018/1058, Oak Ridge National Laboratory, 2019.
[2] AHRTI, Benchmarking Risk Assessment Models and Testing for Flammable Refrigerants (Project 9007-01), Air-Conditioning, Heating & Refrigeration Technology Institute, 2018.
[3] D. Colbourne and Z. X. Liu, R-290 leakage mass flow rate from a refrigerating system, 10th IIR-Gustav Lorentzen Conference on Natural Working Fluids (GL2012). Proceedings. Delft, The Netherlands, June 25-27, 2012
[4] Munson, B. R., Young, D. F., and Okiishi, T. H., 2006, Fundamentals of Fluid Mechanics, John Wiley & Sons, Inc, USA.W
[5] IEC 60335-2-89: Household and Similar Electrical Appliances, Safety: Part 2-89, 2022.